Identification of hydrogen defects in α-Al_2O_3 by first-principles local vibration mode calculations

Jiraroj T-Thienprasert,[1,2] Adisak Boonchun,[1,2] Pakpoom Reunchan,[1,2] and Sukit Limpijumnong[3]
[1]*Department of Physics, Faculty of Science, Kasetsart University, Bangkok 10900, Thailand*
[2]*Thailand Center of Excellence in Physics (ThEP Center), Commission on Higher Education, Bangkok 10400, Thailand*
[3]*School of Physics and NANOTEC-SUT Center of Excellence on Advance Functional Nanomaterials, Suranaree University of Technology, Nakhon Ratchasima 30000, Thailand*
(Received 4 February 2017; published 10 April 2017)

The absorption peaks at $\sim$3200$-$3300 cm^{-1} in α-Al_2O_3 crystal that were previously observed and assigned to hydrogen interstitial were reinvestigated by first-principles local vibration mode calculations. Based on our calculations, we found that the vibration of hydrogen interstitial is not consistent with the observed polarized IR absorption peaks at $\sim$3200$-$3300 cm^{-1} for two reasons: (1) the orientation of the O-H bond is not aligned with the direction of the oscillator observed and (2) the calculated vibrational frequency is much lower than the observed values. The calculated formation energies showed that interstitial hydrogen can strongly bind with aluminum vacancy, forming [H_n-V_{Al}] complex defects. The complexes have the O-H bond in the direction aligned with the direction of the oscillator. The vibration frequencies of the complex defects are also close to the observed value. Therefore, we assign the experimentally observed $\sim$3200$-$3300 cm^{-1} modes to [H_n-V_{Al}] complex defects.

DOI: 10.1103/PhysRevB.95.134103

I. INTRODUCTION

Hydrogen has been reported to be ubiquitous in many materials, especially in metal oxides, and it significantly affects their electrical and optical properties [1–6]. Understanding the fundamental properties of hydrogen impurity in materials is therefore deemed important for modifying physical properties of materials to fit each technological application. Because of its light mass, IR absorption spectroscopy is a powerful tool for probing the location of hydrogen in many materials, especially in metal oxides. The large weight difference between the host atoms and hydrogen impurity generally leads to distinct and localized vibrational modes associated with hydrogen. Molecules containing hydroxyl groups are known to have IR absorption peaks at $\sim$3000 cm^{-1} associated with the stretch-mode vibration of O-H bonds. The O-H bonds in crystals are also vibrated with frequencies somewhat lower than that in molecules but still in the $\sim$3000-cm^{-1} region. However, it is not easy to identify the microscopic structures of hydrogen in crystals solely from the IR peaks because there are many possible configurations for hydrogen to be incorporated. First-principles calculations have been proven as a powerful tool to examine the locations of impurities, in particular light elements such as H, in materials. Many computational studies have been dedicated to the investigation of hydrogen locations in several materials, such as ZnO, SnO_2, TiO_2, and In_2O_3 [1–4,7]. For α-Al_2O_3, which has a rather complex crystal structure, hydrogen impurity has been rather extensively studied experimentally by means of IR absorption spectroscopy [5,8–11]. However, to our knowledge, there are very limited theoretical studies aiming to study the IR signature of hydrogen impurity in α-Al_2O_3 and the origin of the observed IR absorption peaks related with hydrogen impurity are still unclear [12–14].

α-Al_2O_3 is an important material for a variety of applications. For example, it can be used as a substrate for epitaxial growth [15], a surface passivation layer of Si solar cells [16], and a hydrogen permeation barrier [17,18]. In addition, α-Al_2O_3 can be used in optical devices when it is doped with Cr or Ti [19,20]. Generally, the presence of unintentional defects in α-Al_2O_3, such as native point defects and hydrogen, can either degrade or enhance its electrical, mechanical, and optical properties [12,21]. There are several theoretical and experimental studies focusing on the native point defects in α-Al_2O_3 [21–34]. Most of them have been dedicated to the investigation of the origin of the observed photoluminescence spectra, which are mostly assigned to the F-center (oxygen vacancy; V_O) defect. Furthermore, it has been reported that V_O defect in α-Al_2O_3 is the cause of leakage current through the dielectric [21,35]. Beside native point defects, hydrogen is one of the most interesting impurities in α-Al_2O_3 because it can easily diffuse into α-Al_2O_3 and affects its electrical and optical properties. The IR absorption technique has been used to investigate the location of hydrogen. The strong IR absorption peaks at $\sim$3183, 3231, and $\sim$3278 cm^{-1} are observed accompanied by a weak IR absorption peak at $\sim$3309 cm^{-1} [5,8,11]. These vibrational frequencies of $\sim$3200$-$3300 cm^{-1} should relate to the O-H bonding in a crystal as mentioned before. In addition, by using the polarized IR absorption measurements, all vibrational modes associated with the O-H bonds are suggested to lie very close to the basal plane [5,11]. Recently, hydrogen in α-Al_2O_3 has been theoretically studied by first-principles calculations [17]. Zhang *et al.* suggested that hydrogen in α-Al_2O_3 is mainly presented in the form of hydrogen interstitial (H_i^+) defect and some H could exist in the form of substitution for oxygen site (H_O^+) as well as a complex defect between hydrogen and aluminum vacancy (H-V_{Al}) [17]. Moreover, they reported that H_i^+ was suggested to be the predominant diffusion species in α-Al_2O_3 resulting in the low efficiency for protection against H permeation through α-Al_2O_3. More recently, the passivation of C and N impurities by hydrogen in α-Al_2O_3 has been reported [12]. To our knowledge there is no theoretical study which can directly relate the observed vibrational frequencies to the hydrogen locations in α-Al_2O_3 crystal. Therefore, the investigation of the energetics and vibrational frequencies of H-related defects is needed to gain more understanding about the locations of hydrogen impurity in α-Al_2O_3.

In this paper, we performed first-principles density-functional calculations to study the energetics and stability of hydrogen-related defects in α-Al_2O_3. By using the frozen-phonon approximation, we calculated the vibrational frequencies associated with hydrogen-related defects, which could be further used to compare with the observed IR absorption peaks. We propose that the observed IR absorption peaks at $\sim$3200−3300 cm^{-1} are associated with the H_i-V_{Al} complex defects.

II. CALCULATION METHOD

We used first-principles calculations based on spin-polarized density-functional calculations to investigate the H-related defects in α-Al_2O_3. The electron-ion interactions were treated by projector-augmented wave method [36] as implemented in the VASP codes [37,38]. For the exchange-correlation energy, the generalized gradient approximation parameterized by Perdew-Burke-Enrzerhof was employed [39]. The cutoff energy for expanding the plane-wave basis set was set at 500 eV. All atoms in the cell were fully allowed to relax until the Hellmann-Feynman forces [40] became less than 0.01 eV/Å. In this paper, the unit cell of α-Al_2O_3 (corundum) with the hexagonal structure containing 30 atoms was used for bulk calculations. The Monkhorst-Pack scheme [41] with a sampling mesh point of 5×5×5 was used for k-space integrations. The calculated lattice parameters of α-Al_2O_3 are $a = 4.810$ Å and $c = 13.131$ Å in agreement with the experimental values of $a = 4.765$ Å and $c = 13.011$ Å [42]. However, the calculated band gap at the Γ point is only 5.83 eV lower than the experimental band gap of 8.7 eV [43]. This is due to the well-known underestimation in band gap obtained by density-functional calculations.

For defect calculations, a supercell approach with a size of 120 atoms α-Al_2O_3, which is a repetition of the unit cell by 2×2×1, was employed to reduce the spurious defect-defect interactions arising from the neighboring cells. In case of supercell calculations, the k-point mesh was reduced to 1×1×1 shifted from the Γ point. The stability and likelihood of defect formation can then be determined from its formation energy, which is defined by

$$\Delta H_f(D^q) = E_{\text{tot}}(D^q) - E_{\text{tot}}(\text{bulk}) - \sum_X n_X \mu_X + q(E_F + E_{\text{VBM}}) + E_{\text{corr}}, \quad (1)$$

where $E_{\text{tot}}(D^q)$ and $E_{\text{tot}}(\text{bulk})$ are the total energy of a supercell containing the defect D in charge state q and that of a perfect supercell, μ_X is the atomic chemical potential representing an energy required to remove (add) an atom from (to) a supercell to create the defect D, n_X is the number of atom species X being added or removed, q is the charge state of the defect D, E_F is the Fermi energy which is referenced to the valence-band maximum (E_{VBM}), and E_{corr} is the finite-size correction term for charged defects according to the scheme proposed by Freysoldt *et al.* [44,45].

During the growth of α-Al_2O_3 single crystal under thermodynamic equilibrium, the following constraint must be satisfied:

$$E_{\text{tot}}(Al_2O_3) = 2\mu_{Al} + 3\mu_O, \quad (2)$$

where $E_{\text{tot}}(Al_2O_3)$ is the total energy per formula unit of α-Al_2O_3, and μ_{Al} and μ_O are the atomic chemical potentials of Al and O atoms, respectively. To prevent the formation of metallic Al phase in a crystal, μ_{Al} is set to the total energy per formula of metallic Al, and μ_O can be calculated from Eq. (2). This defines the Al-rich growth condition. In the same way, to prevent the existence of O_2 gas in a crystal called O-rich growth condition, μ_O must be set to half of the total energy of O_2 gas and μ_{Al} can be again determined from Eq. (2). In case of hydrogen defect, μ_H is set to half of the total energy of H_2 gas for Al-rich growth condition, while under O-rich growth condition μ_H is determined from $\mu_H = [E_{\text{tot}}(H_2O) - \mu_O]/2$. The latter condition makes our calculations close to the experimental doping condition reporting that the α-Al_2O_3 sample was treated under H_2O vapor [5,8,9].

The vibrational frequencies associated with H-related defects in α-Al_2O_3 are determined by using the frozen-phonon approach [46] within the harmonic approximation. They are further used to compare with the observed IR absorption spectra. The accuracy of the calculated vibrational frequencies

TABLE I. The calculated vibrational frequencies obtained from DFT calculations based on the frozen-phonon approximation compared with the measured vibrational frequencies. The values shown for each species are that of the lowest-energy configuration. The angles shown in the parentheses are measured from the direction of O-H bonding to that of the c axis of the crystal.

Species	Mode	Frequency (cm^{-1})		Error (cm^{-1})
		Calculation	Experiment	
	Symmetric stretching	3722.63	3657 [53]	65.63
H_2O	Asymmetric stretching	3836.30	3756 [54]	80.30
	Bending	1575.49	1595 [53]	−19.51
H_i^{1+}	Stretching	2989.25 (40.1°)		
$[H_1\text{-}V_{Al}]^{2-}$	Stretching	3321.67 (84.7°)		
$[H_2\text{-}V_{Al}]^{1-}$	Stretching	3389.30 (86.4°) 2908.30 (35.5°) 2756.57 (36.3°)	3183, 3231, 3278, and 3309 [5,8,11]	
$[H_3\text{-}V_{Al}]$	Stretching	2822.85 (35.5°) 3375.54 (88.8°)		

via this method can be affirmed by comparing the calculated vibrational frequencies of H_2O to the experimental results as shown in Table I. We found that our calculated vibrational frequencies of both symmetric and asymmetric stretching modes are consistently higher than the observed values by a small amount.

III. RESULTS AND DISCUSSIONS

The electrical and optical properties related with native defects in α-Al_2O_3 have been reported in our previous works [22]. We revealed that the most dominant native point defects are oxygen vacancy V_O, aluminum vacancy V_{Al}, and aluminum interstitial (Al_i) in agreement with an earlier study by Matsunaga *et al.* [26]. In this paper, we aim to identify the sites of H impurity, which are responsible for the observed IR absorption peaks at ~3183, 3231, and ~3278 cm^{-1} [5,8,11]. Based on the polarized IR absorption measurement, the orientations of the oscillator (same direction as the O-H bond) responsible for the observed IR absorption peaks lie very close to the basal plane (or almost perpendicular to the c axis) [5,9,11]. Engstrom *et al.* [11] assigned the peak at ~3278 cm^{-1} to the vibrational mode of hydrogen interstitial, H_i, binding with a host oxygen atom. Therefore, we first examined the stability of H_i defect in α-Al_2O_3. We found that H_i is an amphoteric defect with the defect transition level at $\varepsilon(+1/-1) = 4.19$ eV, as shown in Fig. 1, in agreement with the previous work [17]. Furthermore, we investigated the other feasible forms of H defect and found that H could substitute for the O site forming H_O defect with two defect transition levels at $\varepsilon(+1/0) = 5.67$ eV and $\varepsilon(0/-1) = 6.46$ eV. Remarkably, under Al-rich growth conditions, H_O has a lower formation energy than that of H_i when the Fermi level is in the lower half of the band gap. On the other hand, H_i has the lowest formation energy under O-rich growth condition for all possible Fermi-level values in the band gap. This is because under Al-rich growth condition the formation energy of oxygen vacancy V_O defect is quite low resulting in a high concentration of V_O defect. Consequently, H can incorporate into the vacancy site (H_O) with a low total formation energy. However, under O-rich growth condition, V_O has high formation energy and thus it is more difficult for H_O to form in a high concentration. Other forms of H defect, including H_2, OH, and H_2O defects, were also investigated as shown in Fig. 1. We found that $(H_2)_O$ defect is not stable, i.e., it energetically prefers to split into an isolated H_O and H_i. $(H_2)_i$ and H_2O are neutral defects with quite high formation energy. $(OH)_i$ is an acceptor defect with quite high formation energy except for one specific condition. Under O-rich growth condition and when the Fermi level lies in the upper half of the band gap, $(OH)_i$ has a relatively low formation energy. However, this scenario should not happen in this crystal as described below.

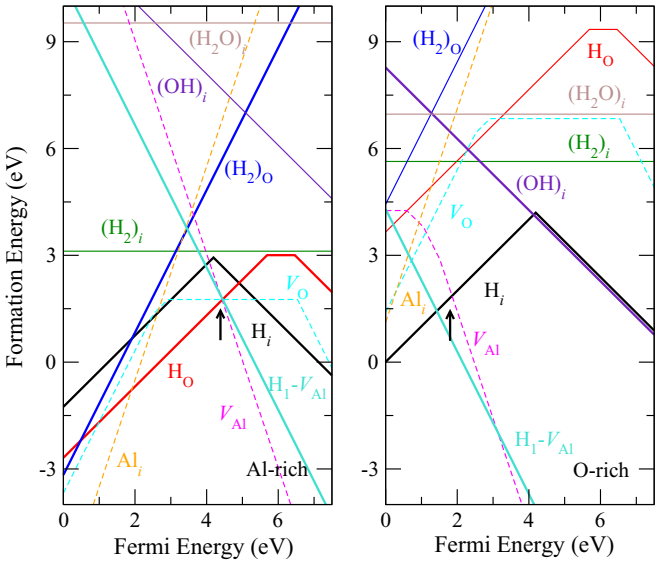

FIG. 1. Formation energies of defects in α-Al_2O_3 as a function of Fermi energy under Al-rich and O-rich growth conditions. The slope of each line indicates the charge state of the defect and the dashed lines represent the formation energy of native defects, including Al_i, V_{Al}, and V_O. The Fermi energy is extended to the special k-point band gap of 7.50 eV.

The pinned Fermi level under Al-rich and O-rich growth conditions can be estimated from the charge neutrality condition: $p\text{-}n + qC(X^q) = 0$, where p and n are the intrinsic hole and electron concentrations, respectively, and $C(X^q)$ is the concentration of defect X in charge state q. Here, the dominant defects X taken into account are H_i, H_O, and V_{Al}. This gives the pinned Fermi level at ~4.46 and ~1.87 eV, above the VBM (see the arrows in Fig. 1) for the Al-rich and O-rich growth conditions, respectively. At the pinned Fermi level, we found that H_O and V_{Al} are the most dominant defects under Al-rich growth condition, while H_i and V_{Al} are the most dominant defects under O-rich growth condition. In the actual measurement, the α-Al_2O_3 sample was doped with H by exposing a sample to H_2O vapor and the IR peaks of ~3200 cm^{-1} associated with the O-H bonding in a crystal were observed [5,9,11]. This experimental setup should place the growth condition close to the O-rich limit where we found that H prefers the H_i form. However, we will show later that H_i could diffuse and then form a complex defect with aluminum vacancy, which is more stable.

Figure 2(b) illustrates the local structure of H_i^{1+} in α-Al_2O_3. Interestingly, the orientation of O-H bonding does not lie on the basal plane but it makes an angle of ~40° with the c axis. This is in inconsistent with the polarized IR measurement that found the 3278-cm^{-1} mode with the oscillator direction ~90° with the c axis [11]. In addition, the calculated vibrational frequency associated with H_i^{1+} is only 2989 cm^{-1}, which is quite low compared to the measured value at 3200 cm^{-1}. Both the structural geometry and the calculated vibration frequency suggested that the H_i^{1+} is not responsible for the observed 3278-cm^{-1} mode. Moreover, there is another experimental measurement that observed the IR absorption peaks at ~2900 cm^{-1} in the α-Al_2O_3 sample, which based on our calculation results could be H_i^{1+} [8].

For the source of the absorption peaks at ~3200 cm^{-1}, we explore other possible H-related defects. As mentioned before, H_i and V_{Al} are the most dominant defects in α-Al_2O_3 crystal. Therefore, H_i could form complex defects with V_{Al}, becoming $[H_n\text{-}V_{Al}]^q$, where n is the number of H attached to the O nearby V_{Al} and q is the charge state of the complexes. To determine the stability of the complex defects, we calculated the binding

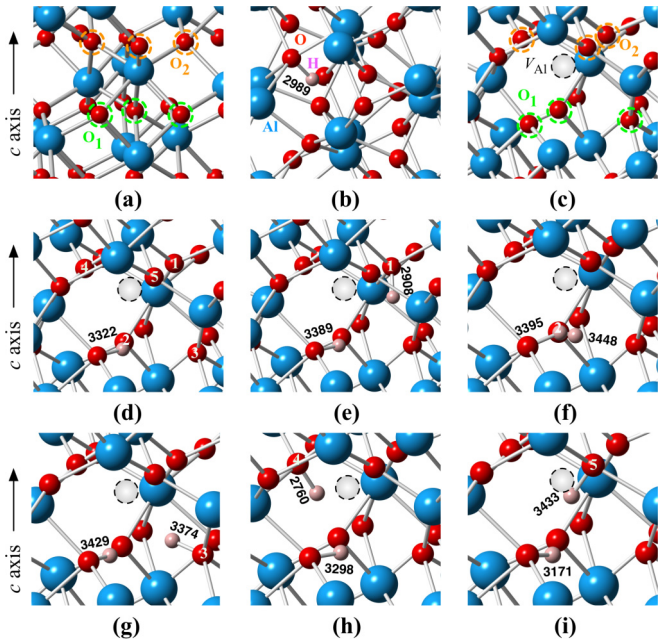

FIG. 2. Local structures of (a) bulk α-Al_2O_3, (b) H_i defect, (c) V_{Al} defect, (d) H_1-V_{Al} complex, and (e)–(i) H_2-V_{Al} complex defects, where second hydrogen is attached to O at site 1 to 5, respectively. The blue, red, and pink spheres represent Al, O, and H atoms, respectively. The values shown in the figure are the calculated vibrational frequencies of the modes associated with those bonds.

energies E_b of the complex defects defined as

$$\begin{aligned} E_b[\mathrm{H}_1 - V_{\mathrm{Al}}] &= \Delta H_f[\mathrm{H}_i] + \Delta H_f[V_{\mathrm{Al}}] \\ &\quad - \Delta H_f[\mathrm{H}_1 - V_{\mathrm{Al}}] \quad \text{for} \quad n = 1, \\ E_b[\mathrm{H}_n\text{-}V_{\mathrm{Al}}] &= \Delta H_f[\mathrm{H}_i] + \Delta H_f[\mathrm{H}_{n-1} - V_{\mathrm{Al}}] \\ &\quad - \Delta H_f[\mathrm{H}_n - V_{\mathrm{Al}}] \quad \text{for} \quad n = 2-3, \end{aligned} \tag{3}$$

where $\Delta H_f[D]$ stands for the formation energy of the defect D. The more positive binding energy, the more formation of complex defect is expected.

In Fig. 2(a), we depict the local structures of bulk α-Al_2O_3, in which each Al atom is surrounded by six O atoms with two inequivalent sites labeled by O_1 and O_2. After removing one Al atom to create V_{Al} defect, the O_1 and O_2 atoms around the vacancy slightly move outward as shown in Fig. 2(c). There are two inequivalent sites for H_i to bind with V_{Al} defect, i.e., at O_1 and O_2 sites. Our calculations show that H_i prefers to bind with V_{Al} at one of the O_1 sites rather than at O_2 with the energy lower by ~0.84 eV. This $[H_1\text{-}V_{Al}]^{2-}$ complex defect is a double acceptor without any defect transition level in the band gap. The formation energy of $[H_1\text{-}V_{Al}]^{2-}$ complex is quite low under both Al-rich and O-rich growth conditions, as shown in Fig. 1. The binding energy of the complex defect is high when the Fermi level is lower than ~5 eV (see Fig. 3) under both Al-rich and O-rich growth conditions, indicating that the complex defect is very stable. In addition, we found that the orientation of the O-H bond in this complex is almost perpendicular to the c axis of a crystal as shown in Fig. 2(d), which is consistent with the orientation of the oscillator of the 3278-cm^{-1} mode observed in the experiment.

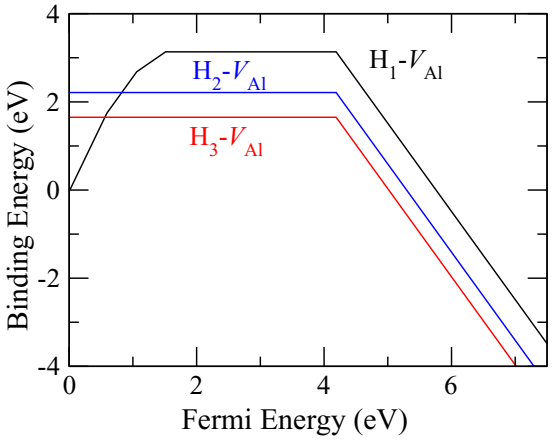

FIG. 3. Illustration of the binding energy as a function of Fermi energy of H-related defects. The positive binding energy indicates a binding of the complex defect whereas the negative binding energy indicates that the complex is unbound.

To compare with the observed IR absorption peaks, we calculated the vibrational frequency associated with the $[H_1\text{-}V_{Al}]^2$ complex defect and the result is shown in Table I. The calculated stretching vibrational frequency of $[H_1\text{-}V_{Al}]^2$ complex defect is ~3321 cm^{-1}, which is in a reasonable agreement with the observed IR absorption peaks at ~3200−3300 cm^{-1}. In order to investigate the feasibility of the complex formation, we further determined the migration barrier of H_i and V_{Al} defects by using density-functional theory (DFT) calculations along with climbing nudge elastic band (cNEB) method [47–50]. We found that H_i could hop from one site to another site in a crystal with the migration barrier of ~0.84 eV, which can be converted to the temperature of ~400 K [51]. This agrees well with a previous theoretical work [17]. For V_{Al} defect, we found that the migration barrier is much higher at ~1.7 eV, meaning that V_{Al} starts to be mobile at a temperature of ~800 K [51]. The rather low migration barrier of H_i indicates that H_i could diffuse throughout the crystal lattice during the growth process and, at some point, form a complex defect with V_{Al} due to a very high binding energy. Our results suggested that V_{Al} could serve as a trap to increase the efficiency for protection against H permeation through α-Al_2O_3. The concentration of V_{Al} can be increased by growing the crystal under O-rich condition.

The high binding energy of $[H_1\text{-}V_{Al}]^{2-}$ complex defect suggests that the complex defect might further bind with another hydrogen to form $[H_2\text{-}V_{Al}]^{1-}$ complex defect. In this case, there are five possible sites for binding the second hydrogen labeled by 1–5 in Fig. 2(d). In Figs. 2(e)–2(i), we illustrate the local structure of $[H_2\text{-}V_{Al}]^{1-}$ complex defect when a second hydrogen binds at sites 1–5. The calculated energy differences among these five configurations are small (with site 1 being the lowest-energy configuration), especially for sites 1–4: the energy difference between sites 1 and 2 (or 3) is only ~0.08 eV and that between sites 1 and 4 is ~0.14 eV. This suggests that a second hydrogen could bind at sites 2–4 as well. The $[H_2\text{-}V_{Al}]^{1-}$ complex is a shallow acceptor without any defect transition level and the binding energy of such complex is quite high when the Fermi level is lower than ~5 eV as illustrated in Fig. 3. By using cNEB method, we

found that a second hydrogen at site 2 or 3 or 4 could migrate to site 1 with the migration barrier of ∼0.44 eV (∼200 K). This means that at room temperature a second hydrogen can migrate, transforming the complex in other configurations to the lowest-energy configuration. To compare with the observed IR absorption peaks, we calculated the vibrational frequencies associated with [H_2-V_{Al}] [1] complex defects for all five configurations depicted in Figs. 2(e)–2(i). The calculated vibrational frequencies of the modes, in which H vibrates almost perpendicular to the c axis, are in good agreement with the observed IR absorption peaks of ∼3200−3300 cm^{-1}. Note that, as a calibrating case, the calculated vibration frequency of the stretch modes of a free H_2O molecule are ∼80 cm^{-1} larger than the observed values as shown in Table I.

Finally, we tested to add another H to $[H_2\text{-}V_{Al}]^{1-}$ complex defect to form a [H_3-V_{Al}] complex defect which is charge neutral. The binding energy of such complex is also shown in Fig. 3 and the calculated vibrational frequencies are listed in Table I. Note that we only show the lowest-energy configuration in this case. The calculated vibrational frequency of H, which vibrates almost perpendicular to the c axis of a crystal, is also close to the observed IR absorption peaks of ∼3200−3300 cm^{-1}. Based on our results, we propose that the vibrational modes of ∼3200−3300 cm^{-1} observed in experiments are from a complex defect between H and V_{Al} defects, not from H_i as previously believed [5,8,11]. Note that Choi *et al.* proposed that oxygen interstitial (O_i) is an important defect under O-rich growth condition [52]. One might speculate the formation of complex defects between O_i and H. In Fig. 1, we explored and found that such complexes, i.e., $(OH)_i$ and H_2O, have high formation energies, making them unlikely to form. In addition, there might exist other impurities in α-Al_2O_3 crystal, such as N, C, Ti, and Fe, which possibly contribute to the observed IR peaks at ∼3200−3300 cm^{-1}. We roughly investigated N_O-H and C_{Al}-H complex defects as reported in Ref. [12] and found that the orientations of N-H or C-H bonding in these complex defects are far away from the basal plane. This suggests that these complex defects do not contribute to those observed IR absorption peaks.

IV. CONCLUSION

Based on first-principles calculations, we identified the microscopic structure of H in α-Al_2O_3 crystal by comparing with the experimentally observed IR modes at ∼3200−3300 cm^{-1}. The experimentally observed modes are previously assigned to H_i^{1+} in α-Al_2O_3. Here, we directly calculated H_i^{1+} in α-Al_2O_3 and found two reasons contradicting the assignment: (1) the orientation of O-H bonding is not close to the basal plane and (2) the vibrational frequency is much lower than the observed value. Based on total-energy calculations, we found that H_i could bind with V_{Al} to form complex defects, which are highly stable. Both the orientation of O-H bonding and vibrational frequencies of these complex defects are consistent with the experimental results. Therefore, the majority of H trapped in a crystal should be in the form of these complex defects. We further suggest that increasing the amount of V_{Al} defect in a crystal could enhance the efficiency of protection against H permeation through α-Al_2O_3.

ACKNOWLEDGMENTS

This research was supported by Kasetsart University Research and Development Institute and Faculty of Science, Kasetsart University. We would like to acknowledge the Synchrotron Light Research Institute, Thailand for the computational resources.

[1] M.-H. Du and K. Biswas, Phys. Rev. Lett. **106**, 115502 (2011).
[2] P. D. C. King, R. L. Lichti, Y. G. Celebi, J. M. Gil, R. C. Vilão, H. V. Alberto, J. P. Duarte, D. J. Payne, R. G. Egdell, I. McKenzie, C. F. McConville, S. F. J. Cox, and T. D. Veal, Phys. Rev. B **80**, 081201(R) (2009).
[3] S. Limpijumnong, P. Reunchan, A. Janotti, and C. G. Van de Walle, Phys. Rev. B **80**, 193202 (2009).
[4] W. M. H. Oo, S. Tabatabaei, M. D. McCluskey, J. B. Varley, A. Janotti, and C. G. Van de Walle, Phys. Rev. B **82**, 193201 (2010).
[5] R. Ramírez, I. Colera, R. González, Y. Chen, and M. R. Kokta, Phys. Rev. B **69**, 014302 (2004).
[6] J. T-Thienprasert, I. Fongkaew, D. J. Singh, M.-H. Du, and S. Limpijumnong, Phys. Rev. B **85**, 125205 (2012).
[7] X. B. Li, S. Limpijumnong, W. Q. Tian, H. B. Sun, and S. B. Zhang, Phys. Rev. B **78**, 113203 (2008).
[8] A. K. Kronenberg, J. Castaing, T. E. Mitchell, and S. H. Kirby, Acta Mater. **48**, 1481 (2000).
[9] R. Ramírez, R. González, I. Colera, and Y. Chen, Phys. Rev. B **55**, 237 (1997).
[10] G. W. Hollenberg, E. P. Simonen, G. Kalinin, and A. Terlain, Fusion Eng. Des. **28**, 190 (1995).
[11] H. Engstrom, J. B. Bates, J. C. Wang, and M. M. Abraham, Phys. Rev. B **21**, 1520 (1980).
[12] M. Choi, A. Janotti, and C. G. Van de Walle, Acs Appl. Mater. Interfaces **6**, 4149 (2014).
[13] A. M. Holder, K. D. Osborn, C. J. Lobb, and C. B. Musgrave, Phys. Rev. Lett. **111**, 065901 (2013).
[14] A. B. Belonoshko, A. Rosengren, Q. Dong, G. Hultquist, and C. Leygraf, Phys. Rev. B **69**, 024302 (2004).
[15] L. Liu and J. H. Edgar, Mater. Sci. Eng. R **37**, 61 (2002).
[16] G. Dingemans and E. Kessels, J. Vac. Sci. Technol. A **30**, 040802 (2012).
[17] G. Zhang, Y. Lu, and X. Wang, Phys. Chem. Chem. Phys. **16**, 17523 (2014).
[18] G. K. Zhang, X. L. Wang, F. L. Yang, Y. Shi, J. F. Song, and X. C. Lai, Int. J. Hydrogen Energ **38**, 7550 (2013).
[19] A. Nehari, T. Duffar, E. A. Ghezal, and K. Lebbou, Cryst. Growth Des. **14**, 6492 (2014).
[20] A. Nehari, A. Brenier, G. Panzer, K. Lebbou, J. Godfroy, S. Labor, H. Legal, G. Cheriaux, J. P. Chambaret, T. Duffar, and R. Moncorge, Cryst. Growth Des. **11**, 445 (2011).
[21] J. R. Weber, A. Janotti, and C. G. Van de Walle, J. Appl. Phys. **109**, 033715 (2011).

[22] T. Watcharatharapong, J. T-Thienprasert, and S. Limpijumnong, Integr. Ferroelectr. **156**, 79 (2014).
[23] V. A. Pustovarov, V. S. Aliev, T. V. Perevalov, V. A. Gritsenko, and A. P. Eliseev, J. Exp. Theor. Phys. **111**, 989 (2011).
[24] T. V. Perevalov, O. E. Tereshenko, V. A. Gritsenko, V. A. Pustovarov, A. P. Yelisseyev, C. Park, J. H. Han, and C. Lee, J. Appl. Phys. **108**, 013501 (2010).
[25] A. I. Surdo, V. S. Kortov, V. A. Pustovarov, and V. Y. Yakovlev, Phys. Status Solidi C **2**, 527 (2005).
[26] K. Matsunaga, T. Tanaka, T. Yamamoto, and Y. Ikuhara, Phys. Rev. B **68**, 085110 (2003).
[27] N. Kristianpoller, A. Rehavi, A. Shmilevich, D. Weiss, and R. Chen, Nucl. Instrum. Methods Phys. Res. B **141**, 343 (1998).
[28] Y.-N. Xu, Z.-Q. Gu, X.-F. Zhong, and W. Y. Ching, Phys. Rev. B **56**, 7277 (1997).
[29] A. Stashans, E. Kotomin, and J. L. Calais, Phys. Rev. B **49**, 14854 (1994).
[30] K. J. Caulfield, R. Cooper, and J. F. Boas, Phys. Rev. B **47**, 55 (1993).
[31] B. D. Evans, J. Appl. Phys. **70**, 3995 (1991).
[32] C. R. A. Catlow, R. James, W. C. Mackrodt, and R. F. Stewart, Phys. Rev. B **25**, 1006 (1982).
[33] K. H. Lee and J. H. Crawford, Jr., Phys. Rev. B **19**, 3217 (1979).
[34] G. J. Dienes, D. O. Welch, C. R. Fischer, R. D. Hatcher, O. Lazareth, and M. Samberg, Phys. Rev. B **11**, 3060 (1975).
[35] D. Liu, S. J. Clark, and J. Robertson, Appl. Phys. Lett. **96**, 032905 (2010).
[36] G. Kresse and D. Joubert, Phys. Rev. B **59**, 1758 (1999).
[37] G. Kresse and J. Furthmüller, Phys. Rev. B **54**, 11169 (1996).
[38] G. Kresse and J. Furthmüller, Comput. Mater. Sci. **6**, 15 (1996).
[39] J. P. Perdew, K. Burke, and M. Ernzerhof, Phys. Rev. Lett. **77**, 3865 (1996).
[40] R. P. Feynman, Phys. Rev. **56**, 340 (1939).
[41] H. J. Monkhorst and J. D. Pack, Phys. Rev. B **13**, 5188 (1976).
[42] H. d'Amour, D. Schiferl, W. Denner, H. Schulz, and W. B. Holzapfel, J. Appl. Phys. **49**, 4411 (1978).
[43] R. H. French, J. Am. Ceram. Soc. **73**, 477 (1990).
[44] C. Freysoldt, J. Neugebauer, and C. G. Van de Walle, Phys. Status Solidi B **248**, 1067 (2011).
[45] C. Freysoldt, J. Neugebauer, and C. G. Van de Walle, Phys. Rev. Lett. **102**, 016402 (2009).
[46] J. T-Thienprasert, S. Limpijumnong, A. Janotti, C. G. Van de Walle, L. Zhang, M. H. Du, and D. J. Singh, Comput. Mater. Sci. **49**, S242 (2010).
[47] D. Sheppard, R. Terrell, and G. Henkelman, J. Chem. Phys. **128**, 134106 (2008).
[48] G. Henkelman, B. P. Uberuaga, and H. Jónsson, J. Chem. Phys. **113**, 9901 (2000).
[49] G. Henkelman and H. Jónsson, J. Chem. Phys. **113**, 9978 (2000).
[50] G. Mills, H. Jónsson, and G. K. Schenter, Surf. Sci. **324**, 305 (1995).
[51] Estimation based on a hopping rate $\Gamma = \Gamma_0 \exp(-\beta E_a)$ of $1/\,\mathrm{min}$, and $\Gamma_0 = 100\,\mathrm{THz}$.
[52] M. Choi, A. Janotti, and C. G. Van de Walle, J. Appl. Phys. **113**, 044501 (2013).
[53] T. Shimanouchi, Tables of Molecular Vibrational Frequencies, Consolidated Vol. 1, NSRDS NBS-39.
[54] K. P. Huber and G. Herzberg, *Molecular Spectra and Molecular Structure. IV. Constants of Diatomic Molecules* (Van Nostrand Reinhold, New York, 1979).